

THE ELASTIC SCATTERING OF 14.2 MeV DEUTERONS BY DEUTERONS AND HELIUM 4 NUCLEI

BY

Hidehiko ITOH

Department Physics, Faculty of Science, Kyoto University

(Received July 11, 1967)

ABSTRACT

The differential cross sections for the elastic scattering of 14.2 MeV deuterons by deuterons were measured at angles between 13.5° and 60° in the laboratory system. The differential cross sections for the elastic scattering of 14.2 MeV deuterons by helium 4 nuclei were also measured at angles between 13.5° and 110° in the laboratory system.

Introduction

The proton-deuteron and neutron-deuteron interactions have been studied by many experimental and theoretical investigators. The study of the d-d interaction is an extension of the study of the p-d and n-d interactions and it gives valuable informations concerning the application of the two-nucleon interactions to heavier nuclear systems. The elastic scattering of deuterons by deuterons has been studied at a number of energies from 0.6 to 10.5 MeV. The differential cross sections in the energy range from 1 to 3.5 MeV were measured by Blair¹⁾ et al. Guggenheimer et al.²⁾ and Allred et al.³⁾ measured the cross section at 7.0 and 10.5 MeV, respectively. In the energy region above 10.5 MeV, an accurate datum has not yet obtained. Since the d-d interaction is much more complicated than the p-d and n-d interactions, the theoretical analysis of the d-d scattering has been dealt with in only a few papers.

A calculation of the cross section at 10 MeV was made by Runge⁴⁾ using Born's approximations. Laskar et al.⁵⁾ applied the resonating formalism to this process.

However, these theoretical calculations fail to agree with the experimental cross sections in the energy region above 6 MeV.

In the energy range below 10.5 MeV, the angular distributions of the d-d scattering do not show any structure, and their cross sections are large in comparison with other scattering processes such as p-p and p-d scatterings. These results are characteristic features of the d-d scattering in this energy region. Therefore, in the energy range above 10.5 MeV, the study of differential cross sections seems to be important.

In the present experiment, an accurate measurement of the differential cross section for the d-d elastic scattering has been performed by using the external 14.4 MeV deuteron beam from the 105 cm cyclotron of Kyoto University. Because the d-He⁴ interaction is expected to be remarkably different from the d-d interaction, the d-He⁴ elastic scattering has been also studied at the same energy.

The theoretical analysis of the experimental results will be reported in elsewhere.

Experimental Procedure

The deuteron beam was bent and focussed, by a system consisting of a pair of quadrupole magnets and a sector-type bending magnet, on a pair of entrance collimators which were placed right front of the 52 cm scattering chamber.

The entrance collimators had circular aperture of 2 mm in diameter and were separated by 25.6 cm. After passing through the collimators, the deuteron beam was led into the scattering chamber and was collected with a Faraday cup which was located behind the chamber and was connected to a current integrator. The whole experimental layout is shown in Fig. 1.

In order to monitor the beam intensity, a cesium iodide scintillation counter was set at the angle of 35° . The pulses from this counter were fed into a 20 channels pulse height analyzer.

At the end of the experiment, the beam energy was measured by using an analyzing magnet.

A target chamber having inner diameter of 10 cm was located at the center of the scattering chamber. The target chamber had a mylar window of $6\ \mu$ thick to minimize the energy loss of emitted particles.

Deuterium gas and helium gas were used as target material. The pressure of the target gas was varied from about 30 cm Hg to 40 cm Hg depending on the experimental conditions. The purity of both gases was 99.97%.

Scattered deuterons were detected by a solid state detector*, whose depletion layer was $500\ \mu$ thick. In order to define the solid angle, a detector slit system was placed in front of the detector. The schematic view of the slit system is shown in Fig. 2 and geometrical dimensions are listed in Table 1.

The pulses from the SSD were amplified by a charge sensitive low-noise amplifier of cascade type and fed into a 1024 channels pulse height analyzer.

Corrections and errors

The errors which are mentioned in this paragraph mean the resultant errors in estimating the differential cross sections due to each origin.

a) The counting loss due to the pulse height analyzer**

The beam intensity was kept constant as much as possible during the experiment ($0.02\ \mu\text{A} \pm 0.001\ \mu\text{A}$). The counting loss due to the 1024 channels PHA whose recovery time was about $50\ \mu$ sec was monitored with a single channel PHA having recovery time of $2\ \mu$ sec.

The errors due to this counting loss were estimated to be less than 1%.

b) The error due to the effect of slit-edge penetration and slit-edge scattering

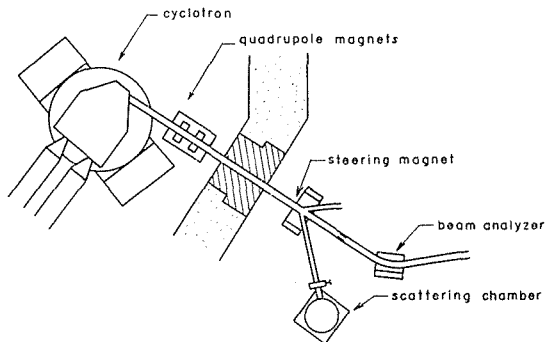
In the case of the scattering experiment using gas target, it is important to evaluate the solid angle defined with the slit system, because the effect of the penetration through the edge and the scattering by the edge of the slit should be taken into account in evaluating the effective solid angle.

i) The slit-edge penetration

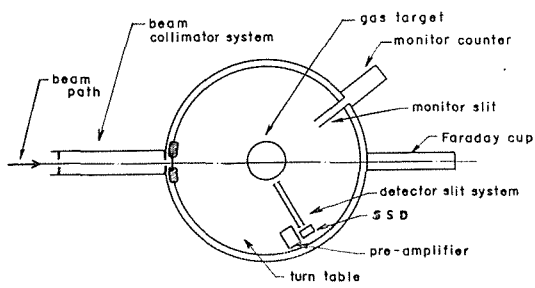
If it is assumed that a scattered deuteron penetrated through the slit-edge

* Hereafter, we abbreviate solid state detector as SSD.

** Hereafter, we abbreviate pulse height analyzer as PHA.



(a)



(b)

Fig. 1. Whole experimental layout.

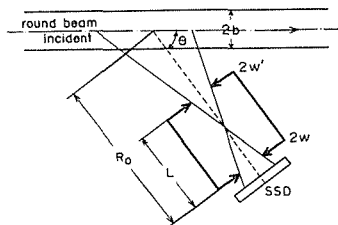


Fig. 2. Schematic view of the slit system.

Table 1. Dimensions of the slit system.

$2w' = 1.068 \pm 0.002$ (unit: mm)
$2w = 1.065 \pm 0.003$
$2h = 3.055 \pm 0.001$
$L = 123.5 \pm 0.005$
$R_0 = 176.0 \pm 0.005$

and reached to the detector as is shown in the Fig. 3. The length L is considered to be shortened by lenth d which denotes the penetrating length for scattered deuterons. The first slit subtends the angle $\alpha = \frac{2w'}{L}$ at a point on the surface of the SSD. When the penetration effect is considered, the angle subtended by the first slit at the same point on the surface of the SSD increases to $\frac{2w'}{L-d}$.

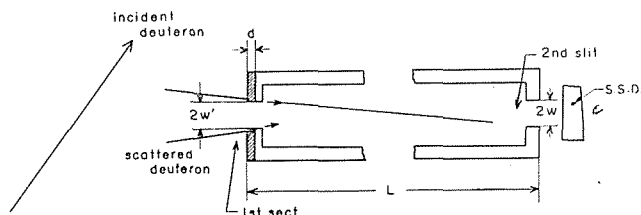


Fig. 3. Illustration of the effects of the slit-edge penetration.

Eq. (1) expresses the increase in the effective target volume, and this increase is caused by the slit-edge penetration. Because the counting rate of the scattered deuterons is proportional to the angle α , the increase of counting rate, ΔC , due to the slit-edge penetration can be expressed as follows:

$$\Delta C = k \left(\frac{2w'}{L-d} - \frac{2w'}{L} \right) \simeq 2w'k \frac{1}{L^2}, \quad d \ll L, \quad (1)$$

where k is a constant.

In the Eq. (1), ΔC is proportional to $\frac{1}{L^2}$.

ii) The slit-edge scattering

Fig. 4 shows the schematic view of the slit-edge scattering. The increase of counts due to the slit-edge scattering, C_s , can be given as follows:

$$C_s = \int_{s=0}^{s=s_{\max}} B N_1 \Delta t_1 \left(\frac{d\sigma_1}{d\Omega} \right)_{\theta_1} \frac{ds \sin(\theta_0 - \theta_1)}{(R_0 - L)^2} \int_{\theta=\theta_{\min}}^{\theta=\theta_{\max}} \int_{\varphi=\varphi_{\min}}^{\varphi=\varphi_{\max}} N_2 \Delta t_2 \left(\frac{d\sigma_2}{d\Omega} \right)_{\theta} \sin \theta d\theta d\varphi \\ + \int_{s'=0}^{s'=s'_{\max}} B N_1 \Delta t_1 \left(\frac{d\sigma_1}{d\Omega} \right)_{\theta'} \frac{ds' \sin(\theta' - \theta_0)}{R_0^2} \int_{\theta'=\theta'_{\min}}^{\theta'=\theta'_{\max}} \int_{\varphi'=\varphi'_{\min}}^{\varphi'=\varphi'_{\max}} N_2 \Delta t_2 \left(\frac{d\sigma_2}{d\Omega} \right)_{\theta''} \sin \theta'' d\theta'' d\varphi', \quad (2)$$

where

$\left(\frac{d\sigma_1}{d\Omega} \right)_{\theta}$: differential cross section for the d-d scattering at the angle θ ,

$\left(\frac{d\sigma_2}{d\Omega} \right)_{\theta}$: differential cross section for the elastic scattering by the material of the slit at the angle θ ,

N_1 : number of scattering nuclei in the target gas per cubic centimeter,

N_2 : number of scattering nuclei in the slit-edge per cubic centimeter,

B : number of incident deuterons,

$\Delta t_1, \Delta t_2$: effective thickness of scattering materials in the target gas and the slit-edge, respectively,

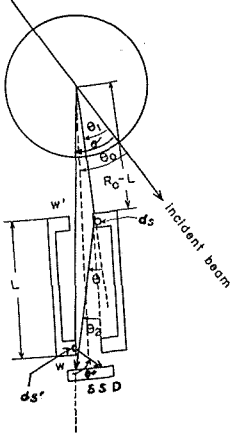


Fig. 4. Illustration of the effect of the slit-edge scattering.

The first and second terms express the slit-edge scattering at the first and second slits, respectively. Because the variation of the angle θ_1 and θ' are very small, $\left(\frac{d\sigma_1}{d\Omega} \right)_{\theta'}$ and $\left(\frac{d\sigma_1}{d\Omega} \right)_{\theta_1}$ can be assumed to be constant. The Eq. (2) is reduced to the Eq. (3).

$$C_s = B N_1 \Delta t_1 \left(\frac{d\sigma_1}{d\Omega} \right)_{\theta_1} N_2 \Delta t_2 \int_{s=0}^{s=s_{\max}} \frac{ds \sin(\theta_0 - \theta_1)}{(R_0 - L)^2} \int_{\theta=\theta_{\min}}^{\theta=\theta_{\max}} \int_{\varphi=\varphi_{\min}}^{\varphi=\varphi_{\max}} \left(\frac{d\sigma_2}{d\Omega} \right)_{\theta} \sin \theta d\theta d\varphi \\ + B N_1 \Delta t_1 \left(\frac{d\sigma_1}{d\Omega} \right)_{\theta'} N_2 \Delta t_2 \int_{s'=0}^{s'=s'_{\max}} \frac{ds' \sin(\theta' - \theta_0)}{R_0^2} \int_{\theta'=\theta'_{\min}}^{\theta'=\theta'_{\max}} \int_{\varphi'=\varphi'_{\min}}^{\varphi'=\varphi'_{\max}} \left(\frac{d\sigma_2}{d\Omega} \right)_{\theta''} \sin \theta'' d\theta'' d\varphi', \quad (3)$$

C_s was found to be less than 1% of the detected counts of the scattering deuterons in the present experiment.

c) The error due to the multiple scattering in the target gases and the window foils of the target chamber

i) The error in the charge collection

The incident beam is multiply scattered in the target gases and the window

foil. These multiple scatterings cause the loss of the beam charge collection. The loss was estimated to be less than 0.4% from Moliere's theory.

- ii) The error due to the in-scattering and out-scattering

As an example, the in-scattering and out-scattering are schematically shown in Fig. 5.

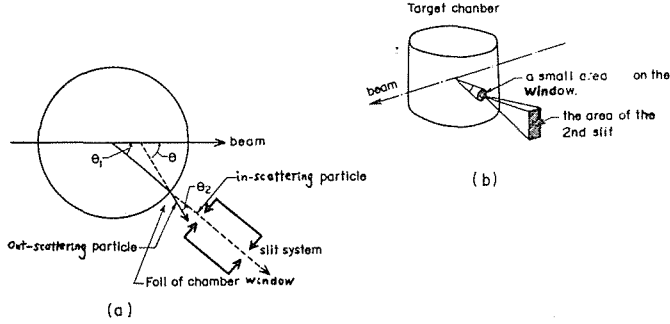


Fig. 5. Illustration of the effects of the in-scattering and out-scattering.

The resultant counts due to the in-scattering and out-scattering are given by the following equation:

$$G = \int_{\theta_1=\theta_{1\min}}^{\theta_1=\theta_{1\max}} \int_{\theta=\theta_{\min}}^{\theta=\theta_{\max}} \int_{\varphi=\varphi_{\min}}^{\varphi=\varphi_{\max}} \left\{ \left(\frac{d\sigma_1}{d\Omega} \right)_{\theta_1} \sin \theta_1 d\theta_1 d\varphi - \left(\frac{d\sigma_1}{d\Omega} \right)_{\theta} \sin \theta d\theta d\varphi \right\} \\ \times BN_1 N_2 \Delta t_1 \Delta t_2 \int_{\theta_2=\theta_{2\min}}^{\theta_2=\theta_{2\max}} \int_{\varphi'=\varphi'_{\min}}^{\varphi'=\varphi'_{\max}} \left(\frac{d\sigma_2}{d\Omega} \right)_{\theta_2} \sin \theta_2 d\theta_2 d\varphi', \quad (4)$$

where

- $\left(\frac{d\sigma_1}{d\Omega} \right)_{\theta}$: differential cross sections for the d-d scattering at the angle θ ,
- $\left(\frac{d\sigma_2}{d\Omega} \right)_{\theta_2}$: differential cross sections for the elastic scattering of deuteron by the window foil at the angle θ ,
- N_1 : number of nuclei per cubic centimeter in the window foil,
- N_2 : number of incident particles,
- $\Delta t_1, \Delta t_2$: effective thickness of scattering material in the target gas and the window foil, respectively,

In order to estimate experimentally the effects of the slit-edge penetration, the slit-edge scattering and the multiple scattering, two slit systems which had different lengths L 's were used. These lengths were 29.75 mm and 123.5 mm. The deuteron spectra which were obtained by using these two slit systems are shown in Fig. 6 and Fig. 7. In these figures, the low energy tails of the elastic peaks in the case of $L=123.5$ mm are remarkably reduced compared to the case of $L=29.75$ mm. The experimental results agree with the numerical estimations, and the total error due to these effects was found to be 0.2%.

- d) The error due to the target density

The gaseous pressure in the target chamber was measured by using a

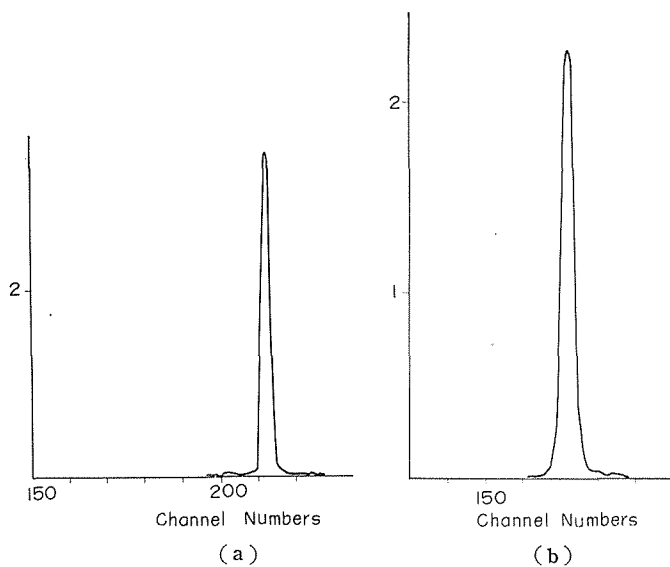


Fig. 6 a) ; b) deuteron spectra measured by using the slit system having $L=123.5$ mm.

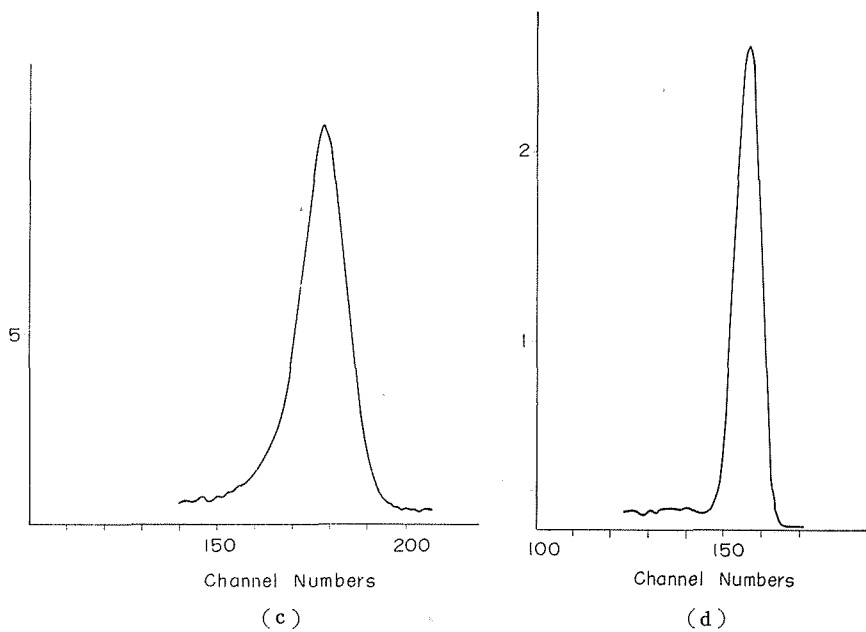


Fig. 7 c), d) deuteron spectra measured by using the slit system having $L=29.75$ mm.

mercury manometer every 30 minutes during the experiment. The temperature of the target chamber was also measured every 15 minutes.

The error due to the evaluation of the target gas density was estimated to be 0.3%.

- e) The error due to the charge collection

The calibration of the Faraday cup and the beam integrator was performed several times during the experiment by using a standard resistor and a battery which calibrated with a potentiometer. The linearity of the beam integrator was guaranteed within 1%.

- f) The background due to target impurities

The deuterium gas used for the present experiment contained the impurity of 0.03%. Although a spectroscopic analysis has not been made to analyze the components of the impurity, the probable impurity may be H,C,O and N. The observed spectra of the SSD also show some corresponding peaks.

- i) Rutherford scattering by carbon, oxygen and nitrogen

The energy difference between the deuterons elastically scattered by carbon and deuterium is larger than 0.6 MeV at the angles of detection.

Therefore, the deuterons from C,N and O were clearly separated from the d-d elastic peak in the observed pulse height spectra as is shown in Fig. 8.

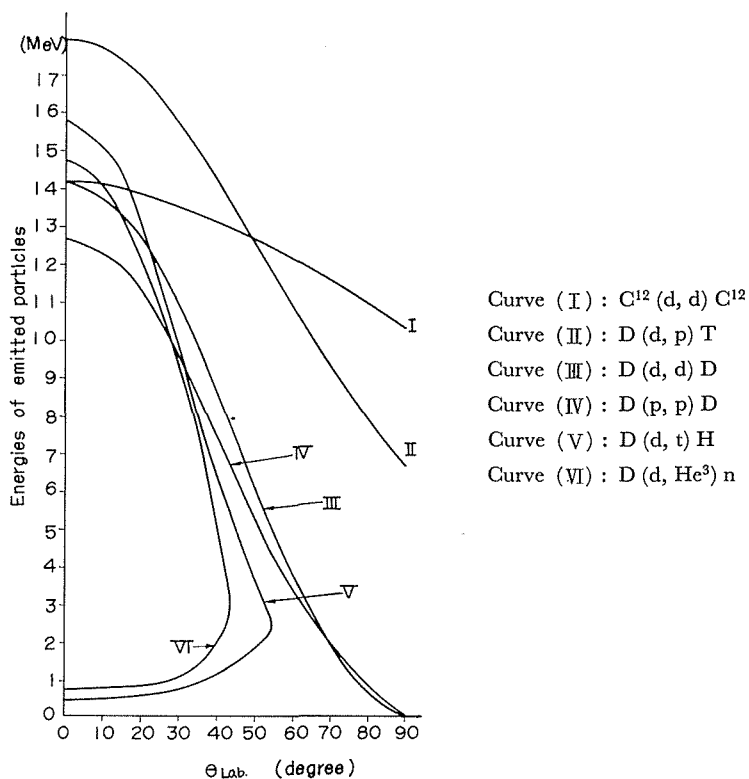


Fig. 8. Energy-angle relations for relevant reactions at the incident deuteron energy of 14.2 MeV,

ii) Rutherford scattering by hydrogen

The energy of deuterons from the elastic scattering by hydrogen is very smaller than the energy of deuteron from the d-d elastic scattering as is shown in Fig. 8.

iii) $D(d,pn)D$

Since the energies of protons from the break-up deuterons are always smaller by the deuteron binding energy than the energy of deuterons from the d-d scattering at the same angle, their influence was negligibly small.

iv) $D(d,p)T$

The energies of protons from the reaction $D(d,p)T$ are larger by about 4 MeV than the energies of deuterons from the d-d scattering.

Since the thickness of the depletion layer of the SSD used in the experiment was not thick enough to stop these protons, the pulse height of the protons should be reduced to about that of the deuterons from the d-d scattering.

The background of these protons amounted to be about 0.5% at forward angles.

e) The background due to the inelastic channels

i) $D(d,t)H$ reaction

Tritons from the reaction $D(d,t)H$ can be separated except at the laboratory angles of 24° and 26° . The triton backgrounds under the deuteron peaks at the laboratory angles of 24° and 26° can be estimated from the total counts of the triton peaks at adjacent angles. The error in estimating the triton background was about 1%.

ii) $D(d,He^3)n$ reaction

The energies of He^3 from the reaction $D(d,He^3)n$ are always lower than the energy of deuterons from the d-d scattering in the angular range above 15° . In addition, energy losses of He^3 in the target gas and the target window are at least 600 KeV. Therefore, the background due to the He^3 was negligibly small in the angular range above 15° . At the angles of 13.5° and 14° , the He^3 background under the deuteron peaks estimated in the same way as case (i).

The energy-angle relations for relevant reactions are shown in Fig. 8.

f) The setting errors of the scattering chamber and the slit system.

The alignment of the scattering chamber and the slit system were performed by using the optical method and Rutherford scattering by Gold. Both results were consistent with each other.

i) The errors due to setting the scattering chamber and the slit system.

The accuracy in evaluating the cross sections due to the setting error of the scattering chamber and the slit system amounted to be 0.4%.

ii) The errors due to the measurement of the dimension of the slit system.

The dimensions of the slit system were measured by using an optical micrometer. The error was estimated to be 0.3%.

g) The error due to monitor counts

The error due to monitor counts was estimated to be 0.25%.

Results

The differential cross sections in the laboratory system were calculated by using Eq. (5)⁶:

$$C = BN_0 \left(\frac{d\sigma}{d\Omega} \right)_{\text{Lab}} \frac{2w2w'}{LR_0 \sin \theta} \left[1 + \frac{w^2 \cot^2 \theta}{3R_0^2} - \frac{w'^2 + w^2}{2L^2} + \frac{b^2}{4R_0^2 \sin^2 \theta} - \frac{3b^2}{8R_0^2} - \frac{h^2}{2R_0^2} \right] \dots, \quad (5)$$

where

C : number of events.

The final results are presented in Tables 2 and 3, in which the cross sections are given in the center of mass system.

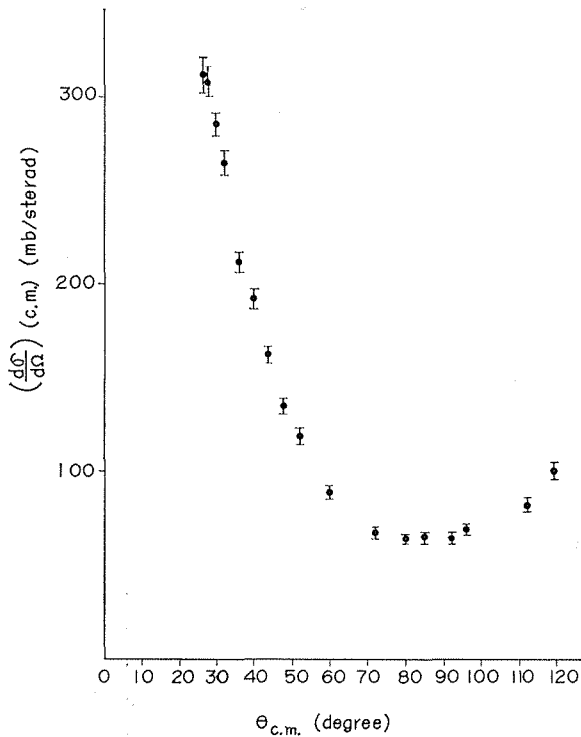


Fig. 9. Angular distribution for the d-d elastic scattering at the incident deuteron energy of 14.2 MeV.

Fig. 9 and Fig. 11 show the angular distributions for the d-d scattering and d-He⁴ scattering, respectively.

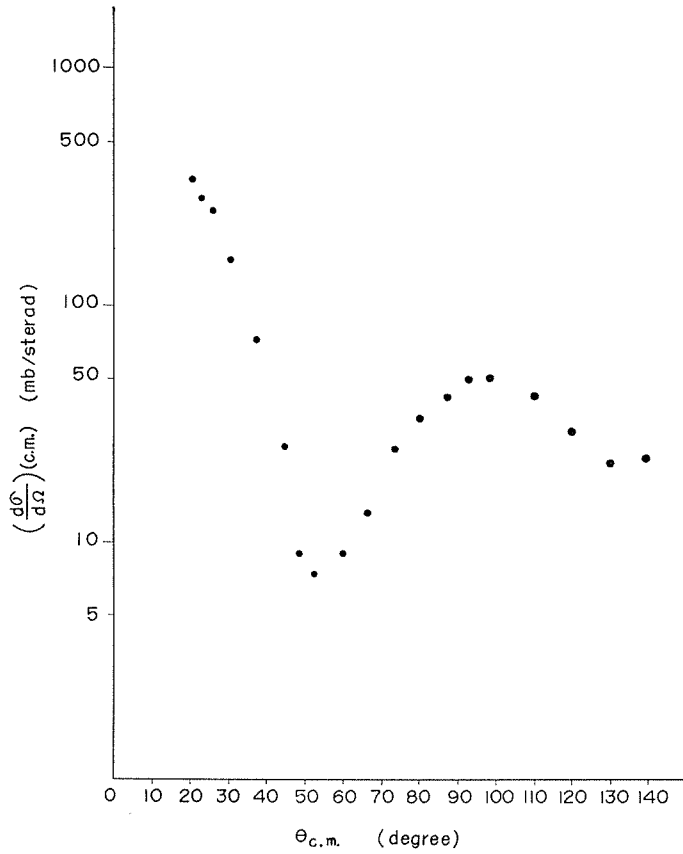


Fig. 10. Angular distributions for the d-He⁴ elastic scattering at the incident energy of 14.2 MeV.

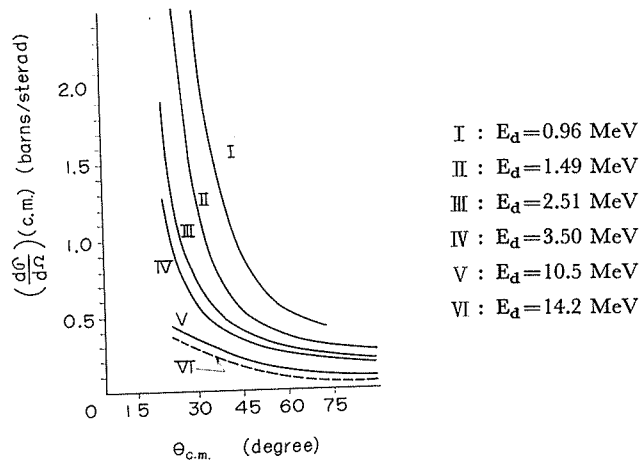


Fig. 11. Energy dependences of angular distributions for the d-d scattering.

Table 2. Numerical results for the d-d elastic scattering at 14.2 MeV. The differential cross sections are given in the center of mass system.

$\theta_{\text{c.m.}}$	$\left(\frac{d\sigma}{d\Omega}\right)_{\text{(c.m.)}}$ (mb/sterad.)	Absolute error (\pm) (mb/sterad.)
27°	312.4	10.0
28°	307.9	9.8
30°	285.1	9.1
32°	265.0	8.5
36°	211.2	7.0
40°	191.5	6.9
44°	162.0	5.7
48°	135.8	4.7
52°	119.3	4.2
56°	101.7	3.5
60°	89.0	3.1
72°	66.5	2.3
76°	66.3	2.3
80°	64.3	2.2
84°	65.4	2.3
88°	64.1	2.2
92°	68.4	2.4
96°	69.1	2.4
112°	81.0	3.0
120°	102.7	3.6

Table 3. Numerical results for the d-He⁴ elastic scattering at 14.2 MeV. The differential cross sections are given in the center of mass system.

$\theta_{\text{c.m.}}$	$\left(\frac{d\sigma}{d\Omega}\right)_{\text{(c.m.)}}$ (mb/sterad.)	Absolute error (\pm) (mb/sterad.)
20°12'	330.7	11.0
22°26'	279.3	8.9
25°25'	247.4	7.9
29°51'	151.2	4.8
37°12'	70.3	2.9
44°29'	25.0	1.2
51°40'	8.6	0.39
58°45'	7.3	0.22
65°42'	13.0	0.48
72°31'	24.8	0.85
79°11'	33.4	1.3
85°40'	40.4	1.4
91°57'	47.7	2.2
98°12'	46.8	2.1
109°30'	41.6	1.7
114°52'	29.2	2.0
129°30'	21.4	1.3
138°12'	22.2	2.4

Acknowledgements

The author wish to express thanks to Prof. S. Yasumi and Prof. T. Yanabu for their continual encouragement. He is also greatly indebted to Prof. K. Miyake, Prof. K. Nishimura and Dr. T. Nakamura for valuable discussions.

Further he is gratefull to the staffs of the Keage Laboratory of Nuclear Science, Institute for Chemical Research, Kyoto University.

REFERENCES

- 1) J.M. Blair et al.: *Phys. Rev.* **74** (1948) 1955.
- 2) K.M. Guggenheimer et al.: *Proc. Roy. Soc. A*, **190** (1947) 196.
- 3) J.C. Allred et al.: *Phys. Rev.* **88** (1952) 431.
- 4) R.J. Runge: *Phys. Rev.* **82** (1952) 1052.
- 5) W. Laskar et al.: *C.R. Acad. Sci., Paris, T.* **246** (1958) 3044~47 and 3158~61.
- 6) J.C. Allred et al.: *Rev. Sci. Inst.* **22** (1951) 191.